Scripta Materialia 140 (2017) 1–4

Contents lists available at ScienceDirect

Scripta Materialia

journal homepage: www.elsevier.com/locate/scriptamat

Regular article

# Critical bending radius of thin single-crystalline silicon with dome and pyramid surface texturing

Jeong-Hyun Woo [a], Young-Cheon Kim [a], Si-Hoon Kim [a], Jae-il Jang [b], Heung Nam Han [c], Kyoung Jin Choi [a,d], Inho Kim [d,e], Ju-Young Kim [a,d,*]

[a] School of Materials Science and Engineering, UNIST (Ulsan National Institute of Science and Technology), Ulsan 44919, Republic of Korea
[b] Division of Materials Science and Engineering, Hanyang University, Seoul 04763, Republic of Korea
[c] Department of Materials Science and Engineering, Seoul National University, Seoul 08826, Republic of Korea
[d] KIST–UNIST Ulsan Center for Convergent Materials, UNIST, Ulsan 44919, Republic of Korea
[e] Center for Electronic Materials, KIST (Korea Institute of Science and Technology), Seoul 02792, Republic of Korea

ARTICLE INFO

*Article history:*
Received 25 May 2017
Accepted 24 June 2017
Available online 3 July 2017

*Keywords:*
Surface modification
Bending test
Solar cells
Finite element analysis
Stress concentration

ABSTRACT

Four-point bending tests are performed on 50-μm-thick single-crystalline silicon (Si) wafers with dome- and pyramid-shaped surface patterns, which are used as flexible Si solar cells. Surface patterns, which act as stress concentrators, reduce the flexural strengths, leading to larger critical bending radius. The critical bending radii of surface-textured Si are much smaller than the calculated values for a single-notch geometry. The finite element analysis shows that the stress concentrations at the tips of the surface patterns effectively disperse in fine and periodic dome and irregular pyramid patterns.



Among the various types of solar cells, crystalline silicon (Si) solar cells are widely used owing to their high energy-conversion efficiency and application feasibility. Recently, thin Si solar cells with a typical wafer thickness of ≤100 μm, which are flexible and possess the advantages of Si solar cells, have been developed. Thin Si wafers are fragile [1]; thus, understanding the critical bending radius is important. Surface texturing of Si wafer has been widely used to reduce reflectivity and enhance light-trapping efficiency [2,3]. However, the textured surface patterns in these Si wafers act as stress concentrators for mechanical deformation, which can reduce the flexibility of thin Si solar cells [4]. The widely used surface texturing in Si wafers is the patterning of irregular pyramids, which is accomplished by chemical etching using potassium hydroxide (KOH) solution in which the etch rates are dependent of the crystallographic orientations of Si [4,5]. Meanwhile, the reflectivity is reduced to approximately 15% due to pyramid surface texturing, and the flexural strength is weakened even in thick Si wafers. On the other hand, thin single-crystalline Si solar cells with surface texturing have been reported to demonstrate higher power conversion efficiency in a bent state and are more durable for cyclic bending [6,7]. When a Si wafer has a single large notch, surface texturing in a fine and periodic array enhances the flexural strength of the Si wafer because the stress concentration at the large notch is effectively dispersed by the surface texturing [8]. The mechanical behavior of thin single-crystalline Si wafers with surface texturing strongly depends on the shape, scale, and distribution of the textured patterns; thus, investigating the effects of surface texturing on the flexibility of thin Si wafers are highly required.

In this study, we perform surface texturing with dome and pyramid shapes on a 50-μm-thick single-crystalline Si wafer. We carry out four-point bending tests on three samples with non-, dome-, and pyramid-textured surfaces. They show elastic bending followed by catastrophic failures. The flexural strengths are analyzed using Weibull distribution, and the critical bending radii are measured. We find that the dome surface texturing has higher flexural strength and smaller critical bending radius than the pyramid surface texturing, whereas the light reflectance is similar to or lower than that of the pyramid-textured sample [9], suggesting that dome pyramid surface texturing is more appropriate for flexible solar cells.

Fig. 1 shows the fabrication procedures of the textured thin Si samples. Both side-polished (100) Si wafers with a thickness of 300 μm were chemically etched in 45 wt% KOH solution at 90 °C from which we obtained 50-μm-thick thin Si wafers, which refers to a flat surface or a non-textured sample. Using the thin Si wafers, we performed surface texturing on the dome- and pyramid-textured surfaces. Fig. 1(a) shows the procedure for the dome-textured surface. $SiO_2$ beads with a diameter of 500 nm, which acted as a hard mask in the subsequent reactive ion etching (RIE) process, were spread on a flat surface in a

* Corresponding author at: School of Materials Science and Engineering, UNIST, Ulsan 44919, Republic of Korea.
*E-mail address:* juyoung@unist.ac.kr (J.-Y. Kim).

http://dx.doi.org/10.1016/j.scriptamat.2017.06.047
1359-6462/

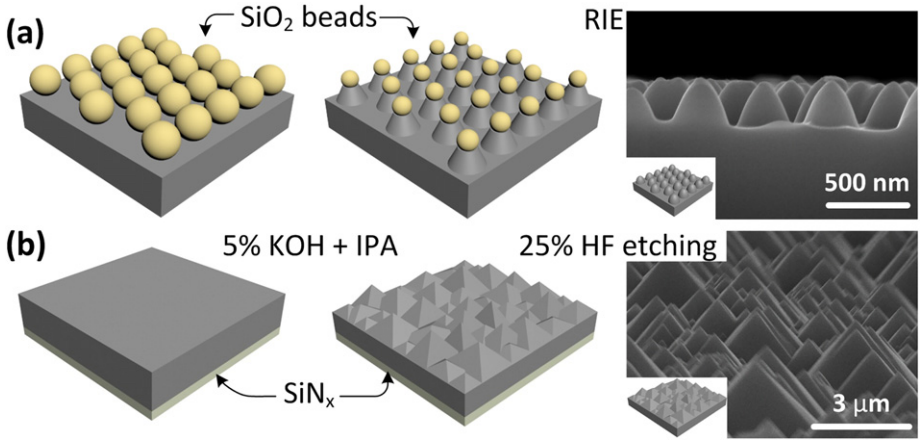


**Fig. 1.** Procedures for (a) dome and (b) pyramid texturing.

packed monolayer by spin coating. This surface was subjected to RIE using $CF_4$ gas and $O_2$ plasma until the $SiO_2$ beads were removed. Nano domes with a height of 300 nm were patterned. To form a pyramid-textured surface, we deposited a 400-nm-thick Si nitride layer as a protective layer at the backside of the wafers using plasma-enhanced chemical vapor deposition and immersed the wafers in 5 wt% KOH and 20 vol% isopropyl alcohol-mixed solution at 70 °C for 30 min. As a result of the anisotropic etch rate of Si in low-concentration KOH solution, randomly distributed pyramids were formed on the surface [5]. Fig. 1(b) shows that the height of the pyramids ranged from 3 to 10 μm. The Si nitride protective layer was removed using a 25 wt% hydrogen fluoride solution. Three samples, namely, non-, dome-, and pyramid-textured samples, were machined in the shape for a four-point bending test with a width of 3 mm and a length of 13 mm using laser scribing. Four-point bending tests were carried out at a loading rate of 2 μm/s, and movie recording was performed using a universal testing machine (Instron 5948). Because of the catastrophic failure of the three samples, at least 30 four-point bending tests were performed for each sample [10].

The stress and strain distributions were analyzed by finite element analysis (FEA). Abaqus 6.12 and Abaqus CAE were used for the FEA simulations and creation of input files, respectively. A two-dimensional deformable shell model was applied, and sample geometries in FEA were designed based on typical cross-sectional scanning electron microscopy (SEM) images of the experimental samples. Young's modulus of 169 GPa and Poisson's ratio of 0.27 were set as the mechanical properties of the Si wafer [11–13].

Fig. 2 shows the Weibull distribution of the flexural strengths, where $P(f)$ on y-axis is the survival probability of a brittle material. Flexural strength $\sigma_f$ is calculated using the following equation:

$$\sigma_f = \frac{3PL}{4bd^2}, \tag{1}$$

where $P$, $L$, $b$, and $d$ are the fracture force, distance of 8 mm between the support spans, sample width of 3 mm, and sample thickness, respectively. Characteristic strength $\sigma_0$ which corresponds to a survival probability of 37% [8,14,15], is 138.5 MPa for the non-textured samples, 103.4 MPa for the dome-textured samples, and 89.8 MPa for the pyramid-textured samples. The characteristic strength of the flexural strength is on the order of non-, dome-, and pyramid-textured Si samples. Surface texturing forms surface notches that act as stress concentrators; thus, the flexural strengths of the dome- and pyramid-textured samples are lower than that of the non-textured sample. Pyramid texturing can likely form sharper and deeper notch than dome texturing, resulting in higher flexural strength of the dome-textured Si sample, which will be discussed in detail later. Weibull modulus $m$ is 3.28 for the non-textured samples, 5.0 for the dome-textured samples, and 5.21 for the pyramid-textured samples. The Weibull modulus corresponds to the magnitude of scattering in the data. A lower Weibull modulus results in wider distribution [16]. The three samples all show elastic bending and catastrophic failure in the four-point bending tests, which means that the flexural strength depends on the highest stress concentrator between the inner spans where identical tensile stress is applied at the surface. The thin Si wafer with a flat surface has the lowest Weibull modulus than the two textured surfaces. This result indicates that the flexural strength of a non-textured sample depends on the probability of containing the highest stress concentrator that is possibly generated in the thinning process by wet etching or wafer growth [8,17,18]. In the other two surface-textured samples, surface texturing most likely provides the highest surface concentrators. The pyramid-textured sample has a higher Weibull modulus than the dome-textured sample, which implies that irregular stress concentrators are introduced at the pyramid-textured surface.

Fig. 3(a) shows typical cross-sectional SEM images of a fracture surface for the dome- and pyramid-textured samples. The dome texturing formed V-shape notches with notch angle $\alpha$ of 75° and tip radius $r$ of 60 nm. $SiO_2$ beads with hard mask RIE for dome texturing were spun-coated in the form of closed-packed monolayer in most areas where periodic domes were formed. In the pyramid-textured samples, V-shaped notches with $\alpha = 70.5°$ and $r = 28$ nm were formed. The size of the pyramids was irregular, ranging from a pyramid height of 3 to 10 μm, and the tip radius was not dependent on the pyramid size. The schematic

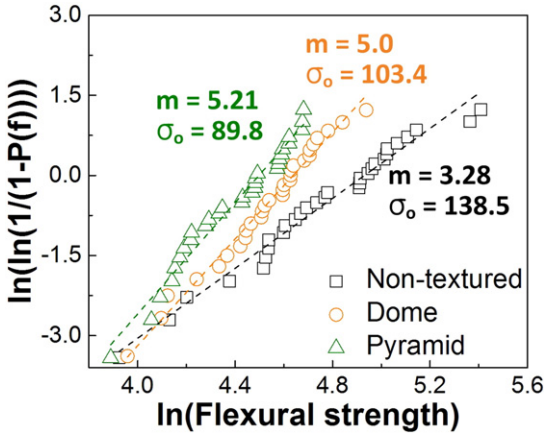


**Fig. 2.** Weibull distribution for flexural strength.

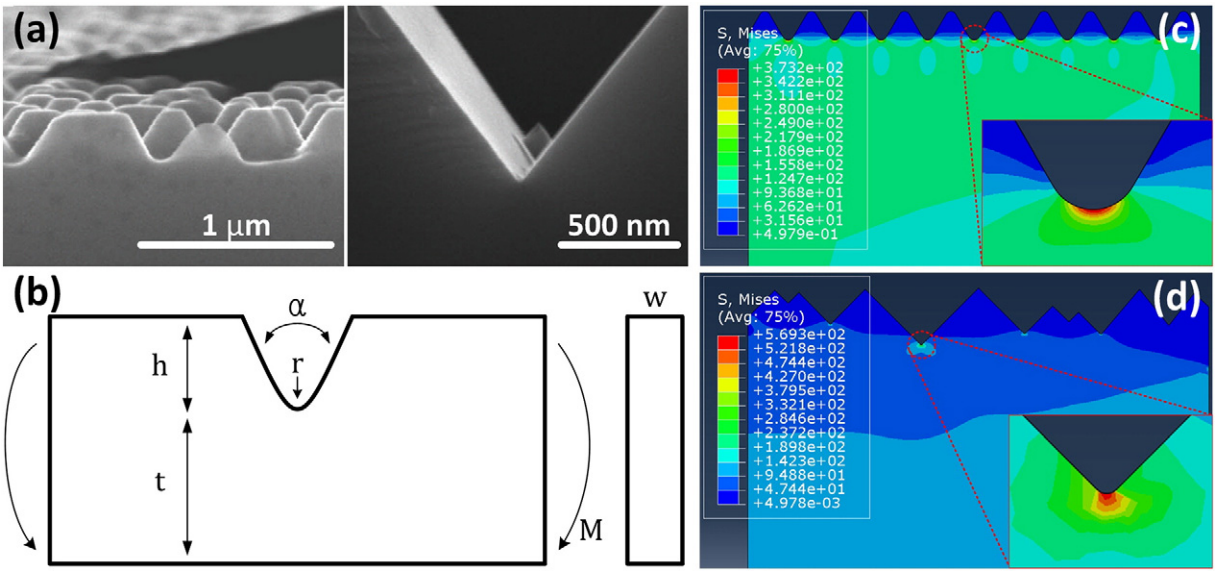


**Fig. 3.** (a) Typical SEM images for fractured cross-sections of dome and pyramid texturing. (b) Schematic for geometry of single notch. Distribution of von Mises stress in two-dimensional (c) dome and (d) pyramid texturing.

of the rectangular parallelepiped with a single notch shown in Fig. 3(b) describes stress-concentration factor $K$ as

$$K = \sigma_{max}/\sigma_{nom}, \tag{2}$$

where $\sigma_{max}$ is the maximum stress at the notch tip and $\sigma_{nom}$ is the nominal stress far from the notch [8], which is expressed as $\sigma_{nom} = 6M/wt^2$, where $M$ is the bending moment, $w$ is the width, and $t$ is the thickness [19]. The measured stress-concentration factors of the dome- and pyramid-textured samples, which were calculated using the ratio of characteristic strength $\sigma_0$ to that of the non-textured sample, were 1.34 and 1.54, respectively. When notch angle $\alpha$ is smaller than 90°, the stress-concentration factors of the U- and V-shaped notches are identical [19], which means that the difference in $\alpha = 75°$ for the dome-textured sample and $\alpha = 70.5°$ for the pyramid-textured samples did not influence the stress concentration at the tips of the surface patterns. The stress-concentration factor for a single U-notch is expressed as

$$K = C_1 + C_2\left(\frac{h}{t}\right) + C_3\left(\frac{h}{t}\right)^2 + C_4\left(\frac{h}{t}\right)^3, \tag{3}$$

where $C_1$ is $0.953 + 2.136\sqrt{h/r} - 0.005(h/r)$, $C_2$ is $-3.255 - 6.281\sqrt{h/r} + 0.068(h/r)$, $C_3$ is $8.203 + 6.893\sqrt{h/r} + 0.064(h/r)$, and $C_4$ is $-4.851 - 2.793\sqrt{h/r} - 0.128(h/r)$ for $2.0 \le h/r \le 20.0$ [19]. In Eq. (3), $h$ is the notch depth as shown in Fig. 3(b). The stress-concentration factor at the tip of a single U-notch with a notch depth of 300 nm and a tip radius of 60 nm, which corresponded to dome texturing, was 5.54 and that with a notch depth of 10 μm and a tip radius of 28 nm corresponding to pyramid texturing is probably >5.54 because it has higher $h/r$ than the dome texturing. However, we did not quantitatively present this because the equation of the stress-concentration factor is valid only up to $h/r = 20$. These values are much greater than the measured 1.34 for dome texturing and 1.54 for pyramid texturing, which can be possibly attributed to the dispersion of stress concentration due to surface texturing. According to previous reports, fine and periodic array of notches more effectively disperse the stress concentration at the highest stress concentrator, resulting in a low stress-concentration factor [20]. Fig. 3(c) shows that the stress-concentration factor calculated using the FEA results for dome texturing is 3.01 and that for pyramid texturing is 4.59. In the FEA simulations, the highest stress concentration was attained at tips of periodic dome patterns simultaneously as shown in Fig. 3(c), and at the tip of the deepest pyramid pattern as shown in Fig. 3(d). The distributions of the von Mises stress show that the stress concentration at the tips of the surface patterns effectively dispersed, depending on the geometries of the neighboring notches, which resulted in lower stress-concentration factors, namely, 3.01 for dome texturing and 4.59 for pyramid texturing, than the theoretical values of a single notch. However, these values were higher than the measured ones, namely, 1.34 for dome texturing and 1.54 for pyramid texturing. Two-dimensional models were used in the FEA simulations, indicating linear notches through the thickness direction in the three-dimensional samples. In the surface-textured samples, domes and pyramids were also distributed along the thickness direction; thus, dispersion of the stress concentration was also effective along the thickness direction. The measured stress-concentration factors of 1.34 for dome texturing and 1.54 for pyramid texturing, which were much lower than the value of the single notch, could be most likely attributed to the effective dispersion of stress concentration in the fine and periodic array of dome patterns and irregular distribution of pyramid patterns.

Fig. 4 shows the critical bending radii of the three samples measured immediately before fracture in the four-point bending test. The critical bending radius was 37.1 (±11.5) mm for the non-textured samples, 46.8 (±14.2) mm for the dome-textured samples, and 59.3 (±17.5) mm for the pyramid-textured samples. The critical bending radius for the dome-textured sample was 26.1% greater than that of the non-textured sample and 26.7% smaller than that of the pyramid-textured sample. The dome-textured sample was more flexible than the pyramid-textured sample. In a previous work, the average reflectance was found to be 32.7% for the non-textured surface, 9.8% for the pyramid-textured surface, and 4.7% for the dome-textured surface in the wavelength range between 700 nm and 900 nm. In this wavelength range, the reflectance of the dome-textured surface was lower than that of the pyramid-textured surface [9]. In terms of the light-trapping effect and mechanical flexibility, dome texturing exhibited better performance than pyramid texturing.

We have measured the flexural strength and bending radius of thin textured Si wafers using the four-point bending tests. From the Weibull analysis, the characteristic strength was 138.5 MPa for the non-textured sample, 103.4 MPa for the dome-textured sample, and 89.8 MPa for the pyramid-textured sample. This result was affected by the stress concentration of the geometries of the textured patterns. With respect to the single-notch concept, the pyramids form deeper and sharper notches than the domes, which induced higher stress concentration and resulted in lower flexural strength. The measured stress-concentration factors of the dome- and pyramid-textured patterns were much lower than the

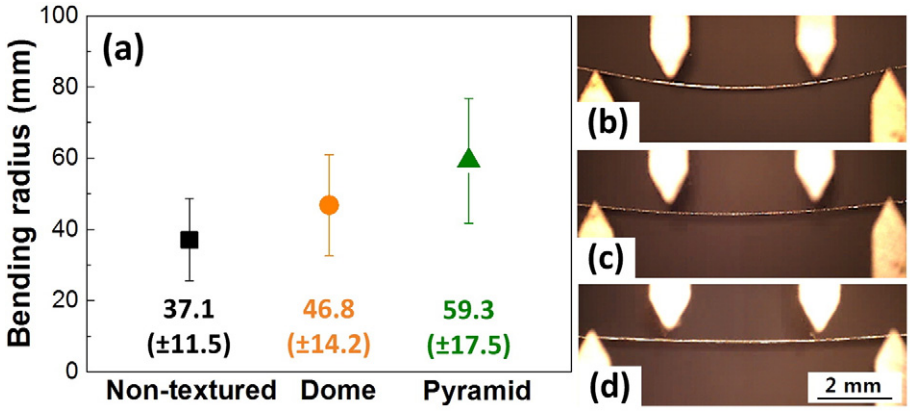


**Fig. 4.** (a) Critical bending radius and typical optical microscope images immediately before fracture in the four-point bending test of (b) non-, (c) dome-, and (d) pyramid-textured Si.

theoretical values of single notches. Through the two-dimensional FEA simulations, we found that dispersion of the stress concentration is more effective in the dome-textured patterns with finer and more periodic surface patterns than the pyramid-textured patterns. The critical bending radii of the non-, dome-, and pyramid-textured samples were 37.1, 46.8, and 59.3 mm, respectively.

## Acknowledgments

This work was supported by the National Research Foundation of Korea (NRF) grant funded by the Ministry of Science, ICT & Future Planning (MSIP) (NRF-2015R1A5A1037627), by the KIST-UNIST partnership program (1.160097.01/2.160482.01), and by the Global Frontier R&D Program on Center for Multiscale Energy System funded by the National Research Foundation under the Ministry of Science, ICT & Future Planning, Korea (2012M3A6A7054855).

## References

[1] O. Borrero-López, T. Vodenitcharova, M. Hoffman, Scr. Mater. 63 (10) (2010) 997–1000.
[2] S. Sánchez de la Morena, G. Recio-Sánchez, V. Torres-Costa, R.J. Martín-Palma, Scr. Mater. 74 (2014) 33–37.
[3] C. Xue, J. Huang, J. Rao, S. Varlamov, Scr. Mater. 92 (2014) 27–30.
[4] J.-S. Lee, S.-W. Kwon, H.-Y. Park, Y.-D. Kim, H.-J. Kim, H.-J. Lim, S.-W. Yoon, D.-H. Kim, Korean J. Mater. Res. 19 (1) (2009) 18–23.
[5] P. Campbell, M.A. Green, Sol. Energy Mater. Sol. Cells 65 (1–4) (2001) 369–375.
[6] C.-C. Lin, Y.-J. Chuang, W.-H. Sun, C. Cheng, Y.-T. Chen, Z.-L. Chen, C.-H. Chien, F.-H. Ko, Microelectron. Eng. 145 (2015) 128–132.
[7] M.M. Tavakoli, Q. Lin, S.F. Leung, G.C. Lui, H. Lu, L. Li, B. Xiang, Z. Fan, Nano 8 (7) (2016) 4276–4283.
[8] K. Kashyap, A. Kumar, C.T. Huang, Y.Y. Lin, M.T. Hou, J. Andrew Yeh, Sci Rep 5 (2015) 10869.
[9] S.-E. Cheon, H.-s. Lee, J. Choi, T.S. Lee, K.-S. Lee, W.S. Lee, W.-M. Kim, H. Lee, D.S. Jeong, Fabrication of Parabolic Si Nanostructures by Nanosphere Lithography and Its Application for Solar Cells, 2017 (unpublished).
[10] B.L. Boyce, M.J. Shaw, P. Lu, M.T. Dugger, Acta Mater. 58 (2) (2010) 439–448.
[11] C.J. Wilson, A. Ormeggi, M. Narbutovskih, J. Appl. Phys. 79 (5) (1996) 2386–2393.
[12] S. Goel, A. Kovalchenko, A. Stukowski, G. Cross, Acta Mater. 105 (2016) 464–478.
[13] T. Vodenitcharova, O. Borrero-López, M. Hoffman, Acta Mater. 60 (11) (2012) 4448–4460.
[14] L. Curkovic, A. Bakic, J. Kodvanj, T. Haramina, Trans. Famena 34 (1) (2010) 13–18.
[15] J. Barredo, V. Parra, I. Guerrero, A. Fraile, L. Hermanns, Prog. Photovolt. Res. Appl. (2013).
[16] I. Paul, B. Majeed, K. Razeeb, J. Barton, Acta Mater. 54 (15) (2006) 3991–4000.
[17] K. Kashyap, Z. Long-Chia, L. Dong-Yan, M.T. Hou, J.A. Yeh, IEEE Electron Device Lett. 36 (8) (2015) 829–831.
[18] K. Kashyap, A. Kumar, C.-Y. Yang, M.T. Hou, J.A. Yeh, 9th IEEE International Conference on Nano/Micro Engineered and Molecular Systems, 2014 390–393.
[19] W.D. Pilkey, Peterson's Stress Concentration Factors, 2008.
[20] M.-K. Yeh, Y.-K. Shao, J.A. Yeh, C. Hsu, Acta Mech. (2015).